Identification and Control of a Nonlinear Soft Actuator and Sensor System

Brian K. Johnson [iD], Vani Sundaram, Mantas Naris, Eric Acome, Khoi Ly [iD],
Nikolaus Correll [iD], *Senior Member, IEEE*, Christoph Keplinger [iD], James Sean Humbert,
and Mark E. Rentschler [iD], *Senior Member, IEEE*

Abstract—**Soft robots are becoming increasingly prevalent, with unique applications to medical devices and wearable technology. Understanding the dynamics of nonlinear soft actuators is crucial to creating controllable soft robots. this letter presents a system identification process and closed-loop control of foldable HASEL (hydraulically amplified self-healing electrostatic) soft actuators. We characterized foldable HASELs with linear frequency response tests and modeled them using a linear superposition of static and dynamic terms. We also identified two responses of the system: an activation and relaxation response. Based on these two responses, we developed a dual-mode controller which was validated through closed-loop control using a capacitive elastomeric strain sensor wrapped around the actuator. Using this integrated sensor, we achieved step response rise times as fast as 0.025 s and settling times as fast as 0.17 s while under load. These system identification and control techniques can be applied to any HASEL-driven soft robot and could be applied to other soft actuators to enable controllable soft robots.**

Index Terms—**Soft sensors and actuators, modeling, control, and learning for soft robots, sensor-based control.**

I. INTRODUCTION

SOFT robotics is a rapidly expanding field [1] with numerous applications to medical devices [2]–[4], wearable technology [2], [5], and human-robot collaboration [6], [7]. The high compliance of soft materials enables new functionalities that are not possible in traditional robotic systems [1], [8].

Brian K. Johnson, Vani Sundaram, Mantas Naris, Eric Acome, Khoi Ly, James Sean Humbert, and Mark E. Rentschler are with the Department of Mechanical Engineering, University of Colorado Boulder, Boulder, CO 80309 USA (e-mail: brian.k.johnson@colorado.edu; vani.sundaram@colorado.edu; mantas.naris@colorado.edu; eric.acome@colorado.edu; khoi.ly@colorado.edu; sean.humbert@colorado.edu; mark.rentsc-hler@colorado.edu).

Nikolaus Correll is with the Department of Computer Science, University of Colorado Boulder, Boulder, CO 80309 USA, and also with the Materials Science and Engineering Program, University of Colorado Boulder, Boulder, CO 80309 USA (e-mail: nikolaus.correll@colorado.edu).

Christoph Keplinger is with the Department of Mechanical Engineering, University of Colorado Boulder, Boulder, CO 80309 USA, and also with the Materials Science and Engineering Program, University of Colorado Boulder, Boulder, CO 80309 USA (e-mail: christoph.keplinger@colorado.edu).

This letter has supplementary downloadable material available at http://ieeexplore.ieee.org, provided by the authors.

Digital Object Identifier 10.1109/LRA.2020.2982056

Developing easily controllable soft actuators is crucial to the viability of these robotic devices. Many types of soft actuators already exist, including electrostatic [9]–[11], fluidic [11], [12], and thermal actuators [13], [14]. A unique form of soft actuator is the HASEL (hydraulically amplified self-healing electrostatic) actuator [15], [16] which is based on electrostatic and hydraulic actuation principles. These actuators exhibit similar performance characteristics to mammalian skeletal muscle, a benchmark for soft actuator performance [16].

Previously, a planar HASEL actuator was modeled and controlled in a closed-loop system using a high-speed camera and capacitive self-sensing [17]. However, this research only modeled the frequency response at a single operating voltage. In addition, the planar HASEL was made from a stretchable elastomer and functioned the same way as laterally stretched dielectric elastomer actuators [18]. Higher performance HASELs have now been created using thin-film polymers [16]; compared to elastomer-based HASEL actuators, these do not require prestretch or mounting to rigid components which simplifies their fabrication and decreases overall weight. The shape of the actuators can also be modified for different modes of actuation [19]. As a result, polymer film-based HASEL actuators with closed-loop control are more practical for a wide range of applications.

This letter provides the first example of system identification and closed-loop control of HASEL actuators made from thin-film polymers. We describe a technique to model the actuator dynamics as a sum of static and dynamic terms using frequency chirp testing at multiple operating points. This model was used to develop an effective feedback controller for the closed-loop system shown in Fig. 1.

Although thin-film HASELs are capable of capacitive self-sensing [16], the technique is highly nonlinear and has variable sensor lag, making it unsuitable for high frequency control. It also requires additional hardware to superimpose the multiple AC signals required for self-sensing. this letter presents an external capacitive elastomeric strain sensor with a simple DC circuit that is integrated onto the actuator for close-loop control.

II. FOLDABLE HASEL DESIGN AND SYSTEM IDENTIFICATION

A. Foldable HASEL Design

The principles of HASEL actuators are well described in previously published works [15], [16], [19]. In summary, HASEL
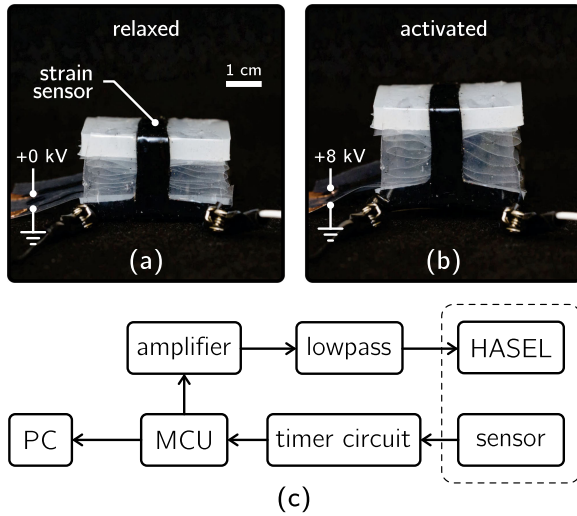
Fig. 1. (a) Relaxed HASEL actuator. The actuator is wrapped with an elastomeric strain sensor, which is shielded from electric fields by dielectric layers. (b) Activated HASEL actuator. Applying high voltage across the electrodes causes an increase in actuator stroke. (c) Hardware for closed-loop control. The output from the strain sensor changes proportional to the increase in stroke and is measured by an LMC555 timer circuit (Fig. 2(c)). The microcontroller unit (MCU) receives measurements from the timer circuit and computes the control output. This is sent to a 5 kV/V high voltage amplifier. The amplified voltage is sent to a 500 Hz low pass filter to reduce noise, and is then applied to the HASEL, causing a change in stroke. The MCU also sends data to a computer (PC) to be logged.

actuators consist of a soft or flexible pouch which is filled with a liquid dielectric. A pair of electrodes are placed on either side of the pouch. When voltage is applied across the electrodes, electrostatic forces displace the liquid dielectric resulting in overall shape change of the pouch. In this work, the pouches are designed to expand linearly when voltage is applied. These pouches are folded and stacked on top of one another to amplify the overall stroke, as shown in Fig. 2.

The fabrication of these foldable HASELs is similar to the process described by Mitchell *et al.* [19]. However, we used a different polymer film for the shell of the actuators. A 20 μm thick polyester (PE) lidding film (L0WS, Multiplastics) was selected because it exhibited less charge retention than biaxially-oriented polypropylene (BOPP) films used in previous works [16], [19]. Charge retention in HASEL actuators, which is related to dielectric absorption in film capacitors, results in HASELs exhibiting changes in maximum and minimum stroke over time when a single polarity high voltage (HV) signal is applied. HASEL actuators made with the PE film exhibited less change in stroke than the BOPP films used in Kellaris *et al.* and Mitchell *et al.* [16], [19]. As a result, we were able to activate HASEL actuators made from PE using a single polarity HV signal which simplified the electronics and controls.

In this work, each stack of foldable HASEL actuators consisted of twelve individual actuators. An actuator consisted of two separate 30 mm × 15 mm pouches, resulting in a 30 mm × 30 mm overall size for an individual actuator. A CNC heat-sealer was made from a commercially available CNC machine (Shapeoko 3 XL, Carbide 3D) fitted with a hot end designed for 3D printers (V6, E3D). The hot end, which consists of a heating

element and extruder tip, was mounted to the z-axis of the CNC machine using a spring-loaded fixture that allows for varying the pressure applied by the extruder tip. Temperature of the extruder tip was regulated using a proportional-integral-derivative (PID) controller (ITC-100, Inkbird). The sealing speed was 450 mm/min, temperature was 195 °C, and sealing pressure was approximately 560 kPa. The pouch electrodes were a conductive carbon ink (CI-2051, Engineered Materials Systems), which were applied using the screen-printing process described by Mitchell *et al.* [19]. The liquid dielectric used was a vegetable-based transformer oil (Envirotemp FR3, Cargill). As described in [19], all twelve actuators were sealed in a single strip. The heat seal pattern included connections between all of the pouches so that all actuators could be simultaneously filled with liquid dielectric. Each actuator consisted of two pouches with 0.38 mL volume of liquid dielectric in in each pouch. After filling, the actuators were then folded in a zig-zag pattern and two small slivers of transfer tape (924, Scotch) were placed on the shell of each actuator to hold the stack together.

To insulate the actuator and mitigate the electric field effects caused by exciting the actuator, we created a silicone rubber dielectric shield. The actuator was sandwiched between two 5 mm-thick blocks of DragonSkin 30 (Smooth-On), covering the top and bottom of the actuator as shown in Fig. 2.

An elastomeric skin was wrapped around the outside perimeter of the dielectric shield. When the actuator stroke increases, the wrap stretches and provides a restorative force to return the actuator to the undeformed state when voltage is removed. The wrap is made of EcoFlex 00–30 (Smooth-On), which is another silicone-based elastomer that exhibits low stress relaxation and good cyclic loading properties [20]. No viscoelastic effects were observed. Additionally, the system identification includes the dynamics of this wrap. The elastomeric strain sensor shown in Fig. 1, described in Section III, is incorporated into this wrap.

B. Experimental System Identification of a Foldable HASEL Actuator

A planar HASEL actuator is a nonlinear time-varying (NLTV) system [21]. We similarly expect foldable HASELs to be NLTV systems, with a single input single output (SISO) relationship between an applied voltage v and the resulting stroke z represented as

$$z = h\left(v(t), t\right), \tag{1}$$

where h is some unknown nonlinear function and t is time. In this letter, we make several assumptions which enable us to approximate the dynamics of a foldable HASEL actuator with a linear time-invariant (LTI) model.

As described in Section II-A, the HASEL is time-varying due to the effects of charge retention. However, we found that the change in stroke due to charge retention was less than 5% during any 180 s duration of any applied voltage between 0-9 kV. We decided to consequently treat the system as time-invariant within time scales of 180 s. Note that although the real system is slowly time-varying, closed-loop control will allow us to counteract the effects of charge retention using integral control. Since we treat
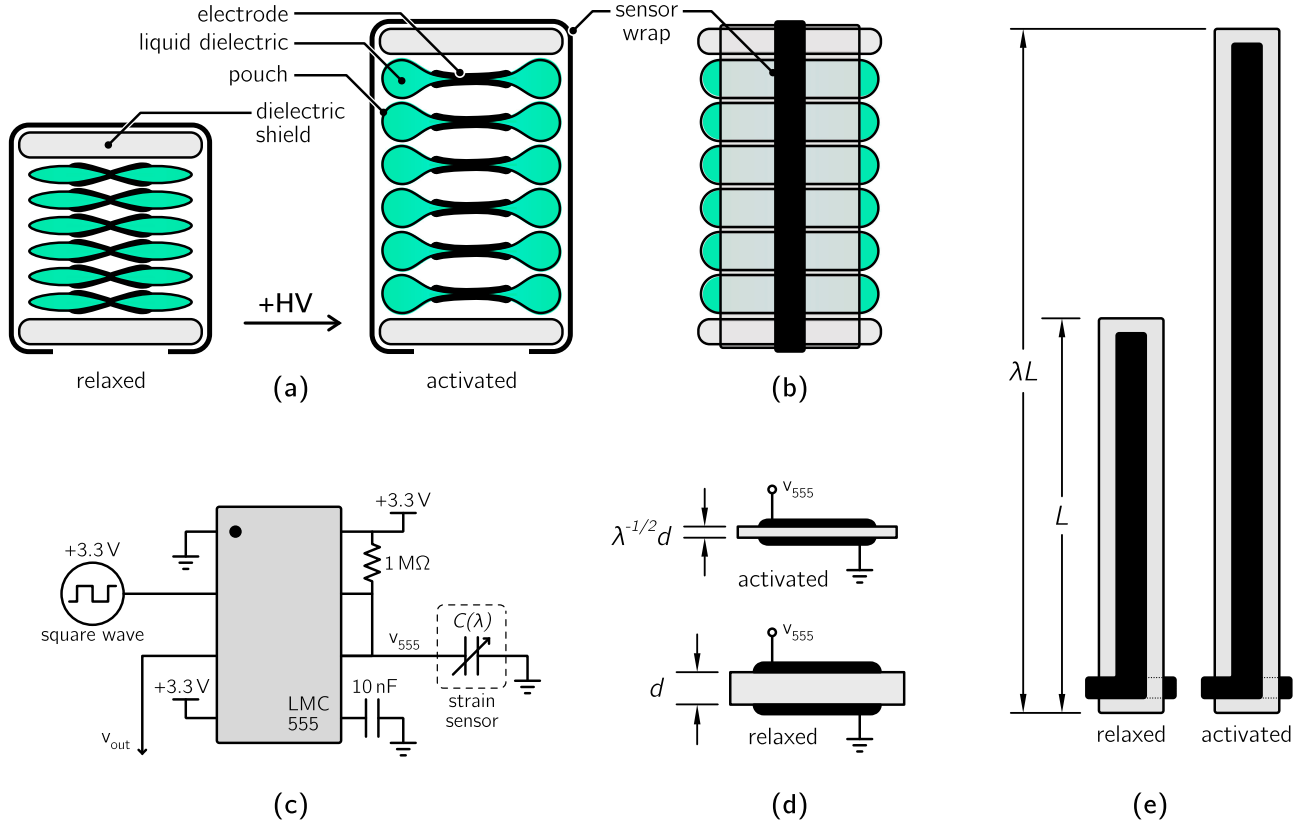
Fig. 2. (a) The foldable HASEL expands upon application of high voltage (HV) to the pouch electrodes. An EcoFlex 00–30 wrap around the outside of the actuator provides a restoring force and contains an integrated strain sensor to measure actuator stroke. Dielectric layers shield the sensor from electric fields generated within the HASEL. (b) Side view of the foldable HASEL with the sensor wrap attached. Fig. 1 also shows this view. (c) Circuit design to transduce capacitance change of the sensor to measured actuator stroke. The LMC555 timer runs in a monostable configuration to relate sensor capacitance $C(\lambda)$ to the duty cycle of v_{out}, which is measured by the MCU. (d) Sensor electrode cross-section. The change in dielectric thickness d is proportional to the sensor stretch ratio λ and causes the change in capacitance $C(\lambda)$. The left electrode is v_{555} at 3.3 V and the right electrode is ground. The dielectric layer is EcoFlex 00–30. **(e)** The stretch ratio λ of the sensor electrodes is proportional to the sensor capacitance $C(\lambda)$, which is measured through the timer circuit.

the system as time invariant, (1) becomes:

$$z = h\left(v(t)\right) \text{ assuming } t \leq 180 \, s. \tag{2}$$

A traditional frequency domain analysis technique [22] is used to experimentally determine a model for foldable HASELs. Typically, these methods utilize zero-mean input signals (e.g. sinusoids) over a range of frequencies so that the system only responds in its dynamic modes. However, a zero-mean signal is not realizable in our system because the actuator stroke is strictly positive. To circumvent this, the system input is calculated using

$$v(t) = v_s + v_d(t), \tag{3}$$

a combination of v_s, a static DC offset voltage, and v_d, a dynamic zero-mean test signal.

Our test signal is a chirp signal, defined as a function of amplitude A (kV), time t (s), and a variable frequency $f(t)$ (Hz):

$$v_d(t) = A\sin\left(2\pi f(t)t\right). \tag{4}$$

A linear chirp is used in which the frequency increases linearly as a function of time. The equation for $f(t)$ is

$$f(t) = \left(\frac{f_f - f_o}{t_{tot}}\right)t \tag{5}$$

where f_o is the start frequency (Hz), f_f is the end frequency (Hz), and t_{tot} is the total test duration (s).

The actuator input is thus a superposition of a step input (the v_s term) and a linear chirp input (the v_d term). We assume the system response stroke z can be similarly separated:

$$z(t) = z_s + z_d(t), \tag{6}$$

where the static term z_s only depends on v_s:

$$z_s = h_s\left(v_s\right), \tag{7}$$

and the dynamic response term z_d depends on some unknown combination of both the static input v_s and the dynamic input v_d:

$$z_d(t) = h_d\left(v_s, v_d(t)\right). \tag{8}$$

To determine the influence of the static input on the dynamic response, we performed frequency response testing using an identical dynamic input v_d at a variety of operating points v_s.

This provided a set of responses:

$$z_1(t) = h_s\left(v_{(s,1)}\right) + h_d\left(v_{(s,1)}, v_d(t)\right)$$

$$z_2(t) = h_s\left(v_{(s,2)}\right) + h_d\left(v_{(s,2)}, v_d(t)\right)$$

$$\vdots$$

$$z_n(t) = h_s\left(v_{(s,n)}\right) + h_d\left(v_{(s,n)}, v_d(t)\right). \tag{9}$$

Subtracting the static $z_{(s,i)}$ term from each response z_i isolates the dynamic responses z_d:

$$z_{(d,1)}(t) = h_d\left(v_{(s,1)}, v_d(t)\right)$$

$$z_{(d,2)}(t) = h_d\left(v_{(s,2)}, v_d(t)\right)$$

$$\vdots$$

$$z_{(d,n)}(t) = h_d\left(v_{(s,n)}, v_d(t)\right). \tag{10}$$

The equivalence of each dynamic response $z_{(d,i)}$ despite variations in their respective static inputs $v_{(s,i)}$, would imply that z_d is fully independent of v_s, and is only a function of the dynamic input v_d. We expect that this also holds for approximation:

$$z_{(d,1)}(t) \simeq z_{(d,2)}(t) \simeq \cdots \simeq z_{(d,n)}(t)$$

$$\Rightarrow z_d(t) \simeq h_d\left(v_d(t)\right). \tag{11}$$

The results described in Section II-B2 and shown in Fig. 3 suggest that v_s indeed has a negligible effect on z_d in the 2–7 kV range, and justify the simplification of our model to the form:

$$z(t) = h_s\left(v_s\right) + h_d\left(v_d(t)\right). \tag{12}$$

In summary, the output stroke of the actuator $z(t)$ is a superposition of the static input response h_s and the dynamic chirp response h_d.

1) Experimental Setup and Test Parameters: We experimentally determined the foldable HASEL model using a data acquisition system (DAQ) (NI 6212, National Instruments), a 5 kV/V high voltage amplifier (Trek Model 50/12, TREK), laser position sensor (LK-H157, Keyence), and a processing script in MATLAB 2019a (MathWorks). Each input signal from (3) was created in MATLAB and sent to the DAQ, which then forwarded the voltage signal to the amplifier. The amplifier applied the high voltage to the actuator, while the laser simultaneously measured the stroke of the top of the actuator. The DAQ returned laser voltage and amplifier voltage to MATLAB.

The form of the input signals was the same as (3) and (4) with signal characteristics are given in Table I. The sample rate for all tests was 10 kHz. The foldable HASELs were characterized using only the elastomeric skin wrapped around the actuator without the dielectric shield included. This was done to create a general model for foldable HASELs that is not dependent on the dielectric shield thickness or material. We separately tested the system including the dielectric shields and observed negligible changes in the frequency response because the mass added by the dielectric layer is minimal.

Our system operating points V_s were 2, 3, 4, 5, 6, and 7 kV, as listed in Table I. The end frequency was selected at 20 Hz. We observed a drastic decrease in stroke amplitude when the
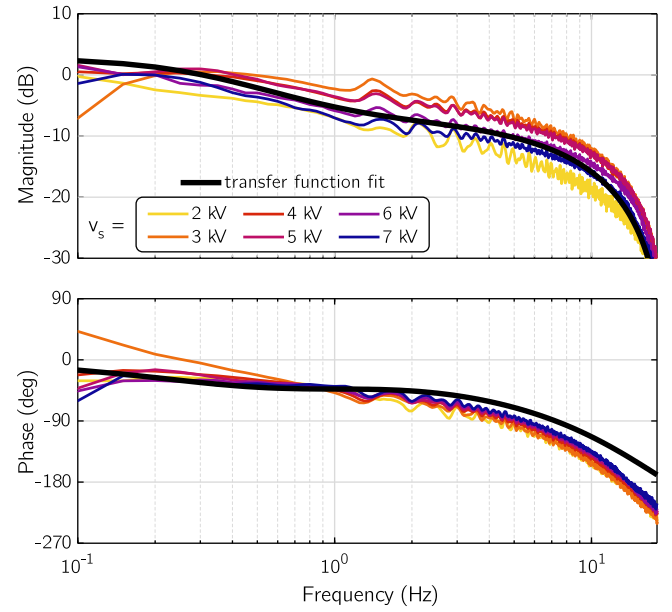

Fig. 3. Bode plot set for a foldable HASEL actuator with elastomeric restoring wrap. Each curve shows the frequency response at 2, 3, 4, 5, 6, and 7 kV static offsets. The offset voltage has negligible effects on the dynamic response between curves. The estimated transfer function fit for this set of curves is also plotted using (17).

TABLE I
CHIRP SIGNAL TEST PARAMETERS

V_s (kV)	A (kV)	f_o (Hz)	f_f (Hz)	t_{tot} (sec)
{2, 3, 4, 5, 6, 7}	1	0.001	20	20

input frequency was greater than 20 Hz so we constrained our analysis up to this limit.

The chirp signal was repeated consecutively for a total of three chirps over 60 s. The goal of the repeated chirps was to account for any effects of charge accumulation; a single 20 s chirp began with low charge accumulation at the start frequency f_0 and greater accumulation near the end of the chirp at f_f. Repeating the chirp allowed us to analyze the low frequency response at higher levels of charge accumulation.

To verify the consistency of the actuator dynamics between actuator copies, we completed one test at each operating point on three similarly-constructed foldable HASELs for a total of 18 tests. Before performing each chirp test, we input a negative 1 kV constant voltage through the HASEL to reverse any accumulated charge from previous tests.

2) Data Processing: After performing these frequency response tests, we processed the amplifier voltage and laser position data in MATLAB. To obtain frequency response data, we took the Fast Fourier Transform (FFT) of both the input (amplifier voltage) and output (laser position measure) using MATLAB's 'fft' function. Dividing the output FFT by the input FFT and then taking the magnitude and phase of the resultant in the real/imaginary plane yielded the complete frequency response of the system.

III. AN ELASTOMERIC STRAIN SENSOR FOR CLOSED-LOOP CONTROL

A. Design of a Capacitive Elastomeric Strain Sensor

We created a capacitive strain sensor to measure the stroke of the foldable HASEL and close the loop on the actuator system. The design of the capacitive elastomeric sensor we describe is similar to others used throughout soft robotics [23]–[25].

The sensor is comprised of two elastomer electrodes with a dielectric material between them, forming a parallel plate capacitor. The dielectric in this sensor is an incompressible elastomer: when the sensor is uniaxially strained, the thickness of the dielectric layer decreases. Using the parallel plate capacitor equation and the fact that the material is incompressible, the change in capacitance of the strained sensor ΔC can be written in terms of only the stretch ratio λ, which is the ratio of stretched length over original length:

$$\Delta C = \frac{\varepsilon_0 \varepsilon \Delta A}{\Delta d} = \frac{\lambda \varepsilon_0 \varepsilon A}{d} = \lambda C_o \qquad (13)$$

where C_o is the pre-strained sensor capacitance, A the original area of the electrodes, d the original distance between electrodes, ε_0 the vacuum permittivity, and ε the dielectric permittivity. The change in capacitance is thus directly proportional to the strain of the sensor.

Since the actuator was already wrapped in Ecoflex 00–30, which is a commonly used sensor dielectric [25], we used the actuator wrap as the dielectric layer for the sensor. This allowed us to relate the change in stroke of the actuator to a change in total capacitance C as the wrap (and sensor) is stretched by a ratio λ. This relationship is shown in Fig. 2(b).

We manufactured conductive electrodes for the sensor in a similar manner to other conductive polymers [25]. We mixed EcoFlex 00–30 with 9 w.t.% carbon black powder (VULCAN-72, Cabot Corp) and 51 w.t.% iso-octane (Sigma Aldrich), which acted as the solvent. To create a degassed, homogeneous mixture, we added 1/4" ball bearings into the mixture container before placing the container in a planetary mixer (ARV-310, Thinky) for seven minutes. The mixer first created a vaccuum during the preliminary mixing stage, then gradually increased the mixing speed from 500 rpm to 1750 rpm. We then blade-casted (ZAA 2300, Zehntner) the mixture onto a 500 μm-thick layer of EcoFlex 00–30 and placed the thin layer into an oven at 70 °C. Once fully cured, the electrodes were laser cut out of the conductive EcoFlex 00–30 sheet and placed on both sides of the dielectric EcoFlex 00–30 layer. Uncured EcoFlex 00–30 was painted over the electrodes to bind the electrodes to the dielectric layer. The total thickness of the sensor was about 800 μm.

An LMC555 timer circuit was used to transduce the capacitance change ΔC into a change in DC voltage, as shown in Fig. 2(c). The LMC555 runs in a monostable configuration, where the duty cycle of the output v_{out} is a function of the capacitor $C(\lambda)$ in the circuit. We used an ARM-based microcontroller unit (MCU) (Teensy 3.6, PJRC) to generate the input signal to the LMC555 at a frequency of 4500 Hz and duty cycle of 89.9%. The MCU measured the rising and falling edges of the output via interrupts, and from the elapsed time between rising and falling edge it transduced the capacitance change.

B. Experimental Verification of Strain Sensor Measurements

We tested the elastomeric strain sensor to validate its use in our closed-loop system. The same experimental setup used to identify the foldable HASEL model described in Section II-B, with the addition of sensor circuitry, was used to determine the sensor model. The sensor was wrapped around the actuator and the dielectric shields, and the sensor electrodes were connected according to the circuit shown in Fig. 2(c).

In the experiment, we sent a set of step inputs – 2, 3, 4, 5, 6, and 7 kV – to the actuator via the high voltage amplifier. The laser then captured the corresponding stroke. The analog voltage outputs of both the sensor and the laser were read by the MCU via a 12 bit ADC and then logged by the computer via serial connection. The sensor measurement was digitally filtered using a second order low pass filter with a cutoff frequency of 40 Hz to reduce noise. The data from one step test are shown in Fig. 4. The results show that the strain sensor has an error less than 5% in steady state and has a high signal-to-noise ratio for closed-loop control. The results also highlight that the foldable HASEL responds different to negative step inputs than positive step inputs; this is discussed further in Section V-A.

IV. CLOSED-LOOP CONTROLLER AND EXPERIMENTAL VALIDATION

A. Hardware for Closed-Loop Control

We closed the loop around a foldable HASEL actuator using the hardware outlined in Fig. 1: an ARM-based MCU (Teensy 3.6, PJRC), a sensor, a low pass filter, a high voltage amplifier, and a foldable HASEL actuator.

The sensor generates a voltage proportional to the HASEL stroke, which is read by the MCU via its onboard 12 bit ADC. The sensor reading is digitally filtered in the MCU using a 40 Hz second order low pass filter to reduce noise, and the filtered signal is then applied to the control algorithm, which will be discussed in Section IV-B. Based on the controller, a desired command voltage is computed and output from the MCU using a built-in DAC. The analog output voltage is then amplified by 5 kV/V. The amplified voltage signal is passed through an analog 500 Hz second order low pass filter to reduce high voltage ripples and is then applied to the HASEL. As the HASEL actuates, the sensor reading changes, and the command voltage updates. The overall frequency of the closed-loop system is 200 Hz.

We first used the laser position sensor as the feedback sensor for closed-loop control. The laser exhibits full linearity to within 16 μm throughout its full sensing range, a repeatability of 0.25 μm, and a sampling rate of over 100 kHz: it can therefore accurately and precisely track a 20 Hz system and thus provided a baseline closed-loop result to easily fine-tune the controller. After performing closed-loop tests with the laser position sensor, we switched the sensor to the integrated strain sensor described in Section III. We then compared the closed-loop control results from both sensing methods.
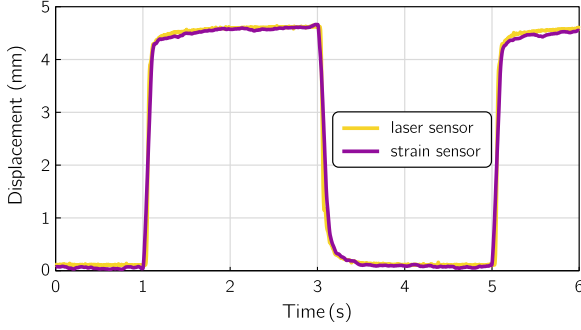
Fig. 4. Strain sensor response to an open-loop actuator step input from 0 to 6 kV. The strain sensor measurement was filtered with a 40 Hz second order low pass filter to reduce noise. It is plotted alongside the measurement from the laser position sensor, which is considered the ground truth for the HASEL stroke. The strain sensor has less than 5% error compared to the laser and is fast enough to capture the step response dynamics. The open-loop step responses also show that the HASEL has two response modes: a fast activation for positive steps (t = 1 s) and a more damped relaxation for negative steps (t = 3 s).

The laser sensor circuit output a voltage proportional to the sensed actuator stroke with a range of 0–3.3 V. The analog sensor signal was converted to a 12 bit integer by the MCU ADC, which was converted into an estimated stroke measurement in mm for the control algorithm. For the laser we used the manufacturer's software (LK-Navigator 2, Keyence) to set this conversion rate to 3 mm/V (e.g. the laser will output 3 V for a HASEL stroke of 9 mm). On the other hand, the capacitance change of the strain sensor corresponds to a change in the duty cycle of the LMC555 timer's output. Two hardware interrupt pins on the MCU were programmed to compute the elapsed time between the falling edge and the rising edge of the LMC555's 4.5 kHz square wave output. The elapsed time, which were directly proportional to the actuator's stroke, was then calibrated using the laser position sensor as ground truth. To map the elapsed time to the displacement, we measured the laser position data and elapsed time at 1 mm step increments from 2–7 mm to determined the line of best fit, relating the strain sensor data to laser position sensor data.

B. Controller Design and Closed-Loop Simulation

As shown in Fig. 4, the actuator behaves differently in an activation (increasing voltage) than relaxation (decreasing voltage) response; we discuss this further in Section V-A. To account for these differences we chose to implement a dual-mode system for feedback control. The block diagram of this dual-mode system is shown in Fig. 5. Reference r is our commanded actuator stroke in mm, which is compared to our sensor measurement $\hat{z}$ and used to calculate error $e = r - \hat{z}$. When $e \geq 0$, the actuator must activate to reach reference position r. When $e < 0$, the actuator must relax to reach r.

To control each response, separate controllers C_+ and C_- were created. We first assumed both controllers to be the same and used the basic form of PID control. The C_+ controller was tuned using a Simulink simulation based on the block diagram in Fig. 5 and the foldable HASEL model we derived shown in (17). We optimized the gains for a fast rise time at the cost of some overshoot. Although the derivative gain is small, we observed
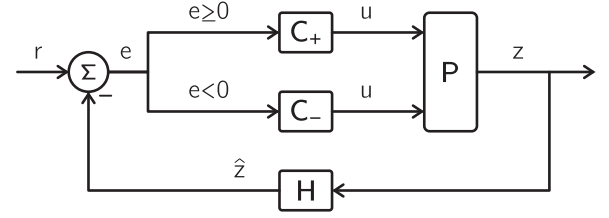

Fig. 5. A dual-mode controller allows separate control of the activation and relaxation responses of the foldable HASEL (plant P). Reference r is the commanded actuator stroke (mm), $\hat{z}$ is the estimated sensor measurement (mm) based on actual stroke z (mm), and u is the control output. The gains of the control switch based on the sign of the error $e = r - \hat{z}$; C_+ is used for $e \geq 0$ and C_- is used for $e < 0$. H represents the sensor used in closed-loop control; we performed closed-loop control using both a laser position sensor and the integrated strain sensor.

an improved overshoot compared to just employing PI control. We then adjusted the C_- controller to achieve the desired step response for HASEL relaxation. Since the relaxation is more damped, C_- is more aggressive than C_+ in order to achieve a faster rise time than the open loop. The final transfer functions for both controllers are given as:

$$C_+(s) = 1.15 + \frac{25}{s} + (1.74 \times 10^{-5})s \qquad (14)$$

$$C_-(s) = 1.25 + \frac{26}{s} + (3.2 \times 10^{-5})s. \qquad (15)$$

These were converted to the discrete-time domain by applying the trapezoidal rule on the integral term and the backward rectangular rule on the derivative term, using a time step of 0.005 s. Taking the inverse z-transform yielded difference equations which we implemented directly on the MCU using Arduino IDE.

C. Closed-Loop Experimental Validation

To validate our actuator model and controller design, we performed real-time closed-loop experiments on the foldable HASEL. Using the test setup described in Section IV-A, shown in Fig. 1, we performed a series of step input tests.

We tested the step response of the foldable HASEL for both positive and negative steps to see the effects of both controllers C_+ and C_-. We expect that the more aggressively designed C_- controller will increase the rise time of the negative step response in comparison to the open loop.

We ran a sequence of positive steps and then negative steps in consecutive order. We ran these tests both for closed-loop control using the laser position sensor and for closed-loop control using the integrated strain sensor. The sequence of stroke commands was as follows (all values in mm):

$$2 \to 4 \to 6 \to 4 \to 2. \qquad (16)$$

The strokes were kept between 2 and 6 mm to avoid saturation of the amplifier voltage. We set a limit of 9 kV on the voltage in order to prevent dielectric breakdown in the HASEL, which may occur in voltages above 9 kV.

In addition, we repeated these steps under strain sensor control while the actuator lifted a 25.5 g load. This load is 64.7% of

TABLE II
CLOSED-LOOP TEST RESULTS

HASEL Mode	Closed-loop Test	10-90% Rise time (s)	5% Settling time (s)	Overshoot (%)
Activation	Open-loop	0.13	0.11	0
	Laser	0.026	0.185	6.0
	Strain Sensor	0.029	0.14	16.0
	25.5 g Load	0.025	0.23	0
Relaxation	Open-loop	0.165	0.275	0
	Laser	0.12	0.17	0
	Strain Sensor	0.071	0.67	5.5
	25.5 g Load	0.12	0.17	0

the total actuator mass of 39.4 g (including dielectric shields). This was done to demonstrate that the closed-loop system can perform work on external loads. The results from all tests are listed in Table II and discussed in Section V-B.

V. RESULTS AND DISCUSSION

A. Foldable HASEL Model

From the frequency response data shown in Fig. 3, we found an anti-resonance at 19.45 Hz and associated drop in phase. Although the physical cause of this is unknown, we determined that a notch filter was a good first approximation. From there, we used a combination of the MATLAB System Identification Toolbox and manual pole/zero placement to arrive at a model for foldable HASELs.

As described in Section II-B1, we observed that the actuator had a more damped step response in relaxation (removal of voltage across the actuator) than in activation (application of voltage). This behavior is shown in Fig. 4. The two modes are likely caused by the driving actuation mechanism within HASELs [16]. The actuator expands when dielectric fluid is displaced by electrodes zipping together, which is a fast process. The actuator contracts only when the dielectric fluid returns to its original location, but without the active force of the zipping electrodes this takes additional time, causing a slower step response in relaxation. However, the two modes are not significantly different, so we modeled the actuator as a single plant transfer function; our dual-mode controller design discussed in Section IV-B accounts for any differences from our model. The resulting foldable HASEL transfer function is:

$$P(s) = \frac{K(s + 50.27)(s + 62.83)(s + 628.3)(s^2 + \omega^2)}{(s + 18.85)(s + 56.55)(s^2 + 230\,s + \omega^2)^2},$$

$$\text{where } K = 10.836, \ \omega = 122.2 \text{ rad/s.} \tag{17}$$

This transfer function maps the actuator input voltage (kV) to an output stroke (mm). The fit of this model is plotted against the frequency response data in Fig. 3.

The data we collected support our conclusion that foldable HASEL responses can be approximated as a sum of independent static and dynamic response components. Although there is not a complete separation of static and dynamic responses, this modeling technique was successful in predicting foldable HASEL dynamics.
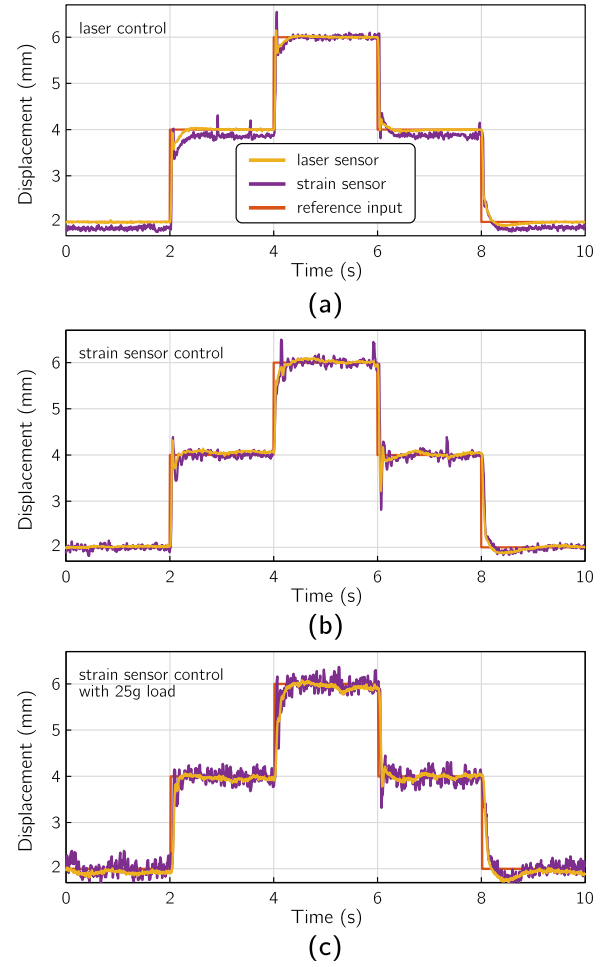

Fig. 6. (a) Closed-loop responses using the laser position sensor. The first two steps show control of the activation actuator dynamics, while the second two steps show control of the relaxation dynamics. The step response is faster than the open loop, and the more aggressive C_- controller for the relaxation response significantly reduced the rise time. Small nonlinearities in the strain sensor calibration resulted in a measurement offset at 2 and 4 mm displacement, though the error remains under 5%. (b) Closed-loop responses using the integrated strain sensor. Closed-loop control using the strain sensor had a higher overshoot and larger settling time compared to the laser position sensor, but still achieved a faster rise time than the open loop. (c) Closed-loop response using the integrated strain sensor under a 25.5 g load, which is 64.7% of the total actuator weight. Under load, closed-loop control was similarly fast.

B. Closed-Loop Control

Closed-loop step responses using the laser position sensor show a faster rise time for both activation and relaxation compared to the open loop responses shown in Fig. 5. The results of both series of tests are summarized in Table II and shown in Fig. 6. The values in Table II represent the best achieved from each test, prioritizing a fast rise time. The results of closed-loop control with the integrated strain sensor show a fast rise time of 0.029 s and 0.07 s for a positive and negative step input, respectfully. These times are 16% slower and 71% faster, respectfully, to those achieved using the laser sensor in closed-loop control. It is not expected that the closed-loop performance using the strain sensor is better than that achieved with the laser sensor; any improved performance is likely due to variability in the physical system and noise.

The strain sensor had a much higher noise level than the laser position sensor. One significant impact of integrating the sensor around the actuator is that the sensor electrodes are subjected to high electric fields due to the voltages used in the HASEL. This was found to significantly increase the noise level of the sensor compared to when it was physically separated from the electric field area. The dielectric shields and the 40 Hz low pass filter helped reduce this noise, but it was not eliminated completely. Another small contributor of noise could be via small vibrations of the actuator which we observed in the laser sensor measurements. However, we found that despite this noise the strain sensor could track actuator strokes as small as 0.1 mm and at frequencies up to 20 Hz. In addition, there was not significant sensor drift over time; the conversion from bits to mm described in Section IV-A remained constant throughout our testing.

VI. CONCLUSIONS

Our work has shown that nonlinear foldable HASEL actuators can be modeled using simple linear frequency response tests. We have demonstrated that the dynamic response of a foldable HASEL is approximately separate from their static response, and that the dynamics are consistent between copies of actuators.

Using this model, we designed a dual-mode PID controller for real-time closed-loop feedback control. We achieved this using an elastomeric strain sensor integrated onto the actuator and benchmarked these results with closed-loop control using a laser position sensor. In both cases, we achieved step responses with faster rise times and settling times compared to the open loop, shown in Table II. We also achieved closed-loop control while under a 25.5 g load, equal to 64.7% the total mass of the actuator, which shows that this system can perform useful work.

Using this actuator model and dual-mode controller, more complex robotic systems driven by foldable HASEL actuators may be controlled. The system identification techniques we utilized may also be applied to other nonlinear soft actuators.

ACKNOWLEDGMENT

REFERENCES

[1] G. M. Whitesides, "Soft robotics," *Angewandte Chemie Int. Edition*, vol. 57, no. 16, pp. 4258–4273, 2018.
[2] M. Cianchetti, C. Laschi, A. Menciassi, and P. Dario, "Biomedical applications of soft robotics," *Nature Rev. Mater.*, vol. 3, no. 6, pp. 143–153, 2018.
[3] E. T. Roche *et al.*, "Soft robotic sleeve restores heart function," *Sci. Translational Medicine*, vol. 9, no. 373, 2017, Art. no. eaaf3925.
[4] X. Yang *et al.*, "Soft artificial bladder detrusor," *Adv. Healthcare Mater.*, vol. 7, no. 6, pp. 1–9, 2018.
[5] T. Q. Trung and N. E. Lee, "Flexible and stretchable physical sensor integrated platforms for wearable human-activity monitoringand personal healthcare," *Adv. Mater.*, vol. 28, no. 22, pp. 4338–4372, 2016.
[6] D. Rus and M. T. Tolley, "Design, fabrication and control of soft robots," *Nature*, vol. 521, no. 7553, pp. 467–475, 2015.
[7] N. Tsagarakis, M. Laffranchi, B. Vanderborght, and D. Caldwell, "A compact soft actuator unit for small scale human friendly robots," in *Proc. IEEE Int. Conf. Robot. Autom.*, Kobe, Japan, May 2009, pp. 4356–4362.
[8] C. Laschi, B. Mazzolai, and M. Cianchetti, "Soft robotics: Technologies and systems pushing the boundaries of robot abilities," *Sci. Robot.*, vol. 1, no. 1, pp. 1–12, 2016.
[9] P. Brochu and Q. Pei, "Dielectric elastomers for actuators and artificial muscles," *Macromol. Rapid Commun.*, vol. 31, pp. 10–36, 2010.
[10] G. Y. Gu, J. Zhu, L. M. Zhu, and X. Zhu, "A survey on dielectric elastomer actuators for soft robots," *Bioinspiration Biomimetics*, vol. 12, no. 1, pp. 1–22, 2017.
[11] S. M. Mirvakili and I. W. Hunter, "Artificial muscles: Mechanisms, applications, and challenges," *Adv. Mater.*, vol. 30, no. 6, pp. 1–28, 2018.
[12] P. Polygerinos *et al.*, "Soft robotics: Review of fluid-driven intrinsically soft devices; manufacturing, sensing, control, and applications in human-robot interaction," *Adv. Eng. Mater.*, vol. 19, no. 12, pp. 1–22, 2017.
[13] C. S. Haines *et al.*, "Artificial muscles from fishing line and sewing thread," *Science*, vol. 343, no. 6173, pp. 868–872, 2014.
[14] F. Sassa and K. Hayashi, "Flexible thermal actuator film for monolithic soft micro robot process," in *Proc. IEEE Sensors*, New Delhi, India, Oct. 2018, pp. 1–4.
[15] E. Acome *et al.*, "Hydraulically amplified self-healing electrostatic actuators with muscle-like performance," *Science*, vol. 359, no. 6371, pp. 61–65, 2018.
[16] N. Kellaris, V. G. Venkata, G. M. Smith, S. K. Mitchell, and C. Keplinger, "Peano-HASEL actuators: Muscle-mimetic, electrohydraulic transducers that linearly contract on activation," *Sci. Robot.*, vol. 3, no. 14, 2018, Art. no. eaar3276.
[17] C. Schunk *et al.*, "System identification and closed-loop control of a hydraulically amplified self-healing electrostatic (HASEL) actuator," in *Proc. IEEE Int. Conf. Intell. Robots Syst.*, Madrid, Spain, Oct. 2018, pp. 6417–6423.
[18] S. J. A. Koh *et al.*, "High-performance electromechanical transduction using laterally-constrained dielectric elastomers part I: Actuation processes," *J. Mechanics Phys. Solids*, vol. 105, pp. 81–94, 2017.
[19] S. K. Mitchell *et al.*, "An easy-to-implement toolkit to create versatile and high-performance HASEL actuators for untethered soft robots," *Adv. Sci.*, vol. 6, 2019, Art. no. 1900178.
[20] J. C. Case, E. L. White, and R. K. Kramer, "Soft material characterization for robotic applications," *Soft Robot.*, vol. 2, no. 2, pp. 80–87, 2015.
[21] N. Kellaris, V. G. Venkata, P. Rothemund, and C. Keplinger, "An analytical model for the design of Peano-HASEL actuators with drastically improved performance," *Extreme Mechanics Lett.*, vol. 29, 2019, Art. no. 100449.
[22] L. Ljung, *System Identification: Theory for the User*. Upper Saddle River, NJ, USA: Prentice-Hall, 1999.
[23] C. Keplinger, M. Kaltenbrunner, N. Arnold, and S. Bauer, "Capacitive extensometry for transient strain analysis of dielectric elastomer actuators," *Appl. Phys. Lett.*, vol. 92, no. 19, 2008, Art. no. 192903.
[24] D. J. Lipomi *et al.*, "Skin-like pressure and strain sensors based on transparent elastic films of carbon nanotubes," *Nature Nanotechnol.*, vol. 6, pp. 788–792, 2011.
[25] M. Amjadi, K. U. Kyung, I. Park, and M. Sitti, "Stretchable, skin-mountable, and wearable strain sensors and their potential applications: A review," *Adv. Functional Mater.*, vol. 26, no. 11, pp. 1678–1698, 2016.